The irreversible structural change in $Mn_{1.1}Fe_{0.9}P_{0.8}Ge_{0.2}$: Evidence for a magnetic driver

Xubo Liu,[1] D. H. Ryan,[1] L. M. D. Cranswick,[2] D. M. Liu,[3] H. G. Zhang,[3] Ming Yue,[3] and Z. Altounian[1]
[1]*Physics Department and Centre for the Physics of Materials, McGill University, 3600 University Street, Montreal, Quebec H3A 2T8, Canada*
[2]*Canadian Neutron Beam Centre, National Research Council Canada, Chalk River Laboratories, Chalk River, Ontario K0J 1J0, Canada*
[3]*College of Materials Science and Engineering, Beijing University of Technology, Beijing 100122, China*

(Presented 3 November 2016; received 18 September 2016; accepted 12 October 2016; published online 27 December 2016)

Neutron powder diffraction measurements complemented by first-principles density functional theory (DFT) calculations have been used to study the irreversible change that accompanies the reversible magnetocaloric transition (MCT) in $Mn_{1.1}Fe_{0.9}P_{0.8}Ge_{0.2}$. We observe the growth and loss of long-period antiferromagnetism as we pass through the MCT for the first time and the development of significant strain in the cycled material. We attribute both the reversible and irreversible changes to the distance dependence of the Mn-Mn exchange in the Mn-P(Ge) *ab*–plane layers. [http://dx.doi.org/10.1063/1.4973287]

I. INTRODUCTION

The current search for solid-state magnetic refrigerants was touched off by the discovery of the $Gd_5(Si, Ge)_4$ system,[1] and since a change in (magnetic) entropy necessarily accompanies any magnetic phase transition, every magnetic material exhibits a magnetocaloric response of some degree. However in order to exhibit a "giant" magnetocaloric effect (MCE) the material needs large moments (to maximise the total entropy), ferro- or at least ferri-magnetic order (so that a modest applied magnetic field can be expected to affect the magnetic transition) and a first-order magnetic transition (so as to concentrate the entropy change in a narrow temperature range). Very many materials have been found to fit the bill to varying degrees.

One such system is the hexagonal Fe_2P-type ($P\bar{6}2m$, #189) $MnFeP_{1-x}(Si, Ge, As)_x$ family.[2,3] These compounds exhibit a significant MCE, as a result of the relatively large manganese moment.[4–6] As with most first-order MCE systems, the magnetocaloric transition (MCT) is a combined structural and magnetic event, and the structural component of the MCT lies at the origin of the 10–20 K hysteresis observed in the MCT. For $MnFeP_{1-x}(Si, Ge, As)_x$ the structural transition takes the form of a large anisotropic expansion of the unit cell at T_C: a increases while c decreases, however the symmetry of the unit cell is unchanged.[7,8]

Remarkably, several members of this compound family exhibit a further, much more extreme hysteresis, often referred to as the "virgin effect": The first passage through the MCT happens at a much lower temperature (by ~50 K) than all subsequent passages[4–6,8–11] and this behaviour can only be re-set by heating to over 1300 K.[10] As this re-set involves heating to well above the ~200 K magnetic transition, it cannot be magnetic in origin and must therefore reflect a structural change in the material, however this change in structure clearly survives the structural cycling associated with the MCT and a previous structural search was unable to determine the nature of this change.[4]

We report here on a neutron powder diffraction study of $Mn_{1.1}Fe_{0.9}P_{0.8}Ge_{0.2}$ which is a follow-up on our earlier Mössbauer spectroscopy work[6] where we found evidence for a significant shift in the

MCT between first and subsequent coolings in this material. We observe a previously unreported magnetic signature associated with the first pass through the MCT and note a significant increase in the diffraction linewidth on cycling. We supplement the experimental work using first-principles density functional theory (DFT) calculations to develop some insight into the origins of the structural instability.

II. EXPERIMENTAL METHODS

A polycrystalline sample with a nominal composition of $Mn_{1.1}Fe_{0.9}P_{0.8}Ge_{0.2}$ was prepared by a ball milling plus spark plasma sintering (SPS) process.[12] The starting materials were Mn powder (99.99 wt.%), Fe powder (99.99 wt.%), red P powder (99.3 wt.%) and Ge powder (99.99 wt.%). The crystal structure was checked by x-ray powder diffraction with a Cu-K_α radiation at room temperature.

Neutron powder diffraction experiments were carried out on the C2 multi-wire powder diffractometer (DUALSPEC) at the NRU reactor, Canadian Neutron Beam Centre, Chalk River, Ontario. The neutron diffraction data were collected as a function of temperature for $4^\circ \leq 2\theta \leq 84^\circ$ at a wavelength of 2.3721 Å. Additional patterns were collected at 300 K and 4 K at a wavelength of 1.3306 Å. All diffraction patterns were refined using the GSAS/EXPGUI suite of programs.[13,14]

The inter-site exchange coupling parameters J_{ij} of the Heisenberg model have been derived from DFT electronic structure calculations and a linear-response method[15] and implemented in LM code.[16–18] We adopt a Green's function technique combined with the linear muffin-tin orbital (LMTO) method with atomic sphere approximation (ASA). In this approach, exchange interactions are calculated as the response to small-angle fluctuations of the spin orientations.

III. RESULTS AND DISCUSSION

Room temperature x-ray and neutron diffraction confirmed that $Mn_{1.1}Fe_{0.9}P_{0.8}Ge_{0.2}$ crystallises in the hexagonal Fe_2P-type structure with space group $P\bar{6}2m$ (#189) with a small amount (<3 wt.%) of MnO. The lattice constants are a=6.0384(1) Å and c=3.4683(1) Å. Rietveld analysis of the room temperature neutron diffraction pattern indicates that the Mn atoms fill the 3g site $(0.595(1),0,\frac{1}{2})$ and 13.6(3)% of the 3f site (0.253(1),0,0) while the Fe atoms occupy the rest of the 3f site in addition to a very small amount (6.0(3)%) of Fe entering the 3g site. P and the Ge atoms, within experimental error, randomly occupy the 2c and 1b sites. No particle size broadening was observed in the diffraction patterns of the as-cast material so they were treated as "bulk" in the subsequent analysis.

On cooling through the MCT, neutron powder diffraction shows that $Mn_{1.1}Fe_{0.9}P_{0.8}Ge_{0.2}$ changes from the paramagnetic $\alpha-$phase to the ferromagnetic $\beta-$phase. This process is marked by the appearance and growth of many new diffraction peaks at the expense of those from the $\alpha-$phase. The anisotropic change in lattice parameters on going from $\alpha \rightarrow \beta$ is clearly visible in Figure 1 as the a–axis expands by ~2.3% while the c–axis contracts by ~4%.

It is evident from Figure 2 that the $\alpha \rightarrow \beta$ conversion is incomplete, and 14.8(3) wt.% of the $\alpha-$phase remains, even at 4 K, consistent with previous reports for this system.[19] This persistence of the $\alpha-$phase below the MCT affords us an opportunity to study its behaviour as it too orders magnetically at the MCT.[6] The anisotropic changes in the $\alpha-$phase lattice parameters, are both smaller than those in the $\beta-$phase and of the opposite sign: The a–axis exhibits a marked contraction, while the c–axis expands slightly. These changes in the $\alpha-$phase are clearly tied to the MCT as they exhibit the same shift after the first cycle and also the same heat/cool hysteresis (this is more obvious in the a–axis data in Figure 1). These observations point to there being a permanent (at least below 300 K) change in the $\alpha-$phase that is induced by the first cooling.

While the ~20 K hysteresis between the first heating and second cooling is apparent in Figure 2, the more significant observation from Figure 2 (also visible to a lesser extent in the lattice parameters shown in Figure 1) is that the $\alpha \rightarrow \beta$ conversion occurs ~55 K later on the first cooling cycle than it does on the second (and all subsequent) cooling cycles. This shift in the MCT between the first and subsequent cycles has been noted in a number of $MnFeP_{1-x}$(Si, Ge, As)$_x$ compounds[4–6,8–11]

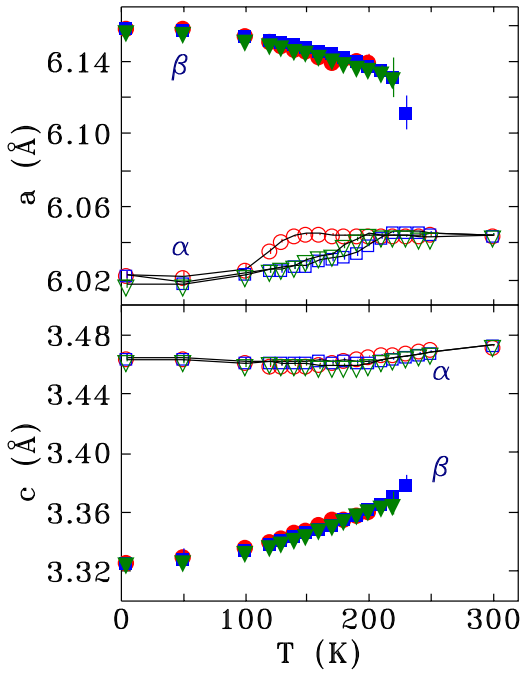

FIG. 1. Temperature dependence of the lattice constants (a, top and c, bottom) for the α and β phases during thermal cycling of $Mn_{1.1}Fe_{0.9}P_{0.8}Ge_{0.2}$. Circles (red), squares (blue) and triangles (green) are for the first cooling, first warming and second cooling process. Open and solid symbols are for α and β phases, respectively.

but its origins have eluded investigation so far. Analysis of neutron diffraction patterns taken at 300 K (*i.e.* in the $\alpha-$phase) reveals no statistically significant differences in the lattice parameters, Fe/Mn site occupations or atomic positions. A similar conclusion was reached in a neutron diffraction study of $MnFeP_{0.6}Si_{0.4}$.[4] However subtracting the diffraction pattern of the cycled material from that obtained before cooling *does* reveal a difference: The diffraction peaks from the cycled material are clearly broader (see Figure 3). Fitting the modified line profile for the full diffraction pattern (both wavelengths) yields a strain of 0.13(1)%. This suggests that while the average atomic positions do not change, there are significant random displacements that occur during the first cooling cycle that persist as the material returns to the $\alpha-$phase, and do not anneal out at 300 K. They appear to survive unless heated to ~1300 K.[10]

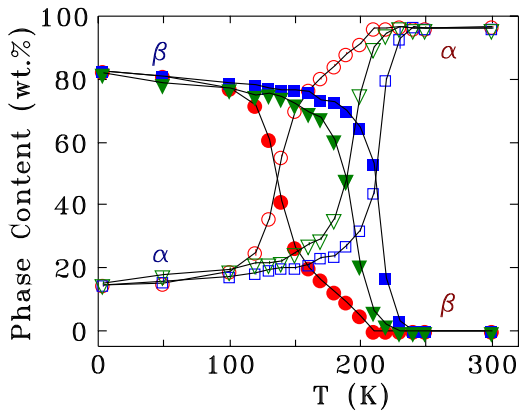

FIG. 2. Temperature dependence of the fraction of the α and β phases in $Mn_{1.1}Fe_{0.9}P_{0.8}Ge_{0.2}$ during the thermal cycles, derived from the neutron diffraction data. Circles (red), squares (blue) and triangles (green) are for the first cooling, first warming and second cooling process. Open and solid symbols are for α and β phases, respectively.

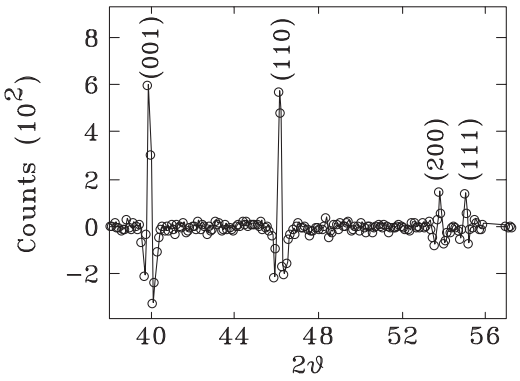

FIG. 3. Difference between the 2.3721 Å neutron diffraction patterns taken for the as-made and cycled $Mn_{1.1}Fe_{0.9}P_{0.8}Ge_{0.2}$ taken at 300 K. The form of the difference pattern clearly indicates that the lines have broadened on cycling.

Treating the broadening as a particle size effect returns ~5000 Å crystallites, but does not yield an improved fit over the strain-based analysis. We observed no tendency for the material to break up on cycling as might be expected if the grains were being reduced in size, nor is it clear how a modest reduction in grain size might lead to the observed MCT irreversibility in this system. We therefore prefer the strain model.

At a neutron wavelength of 2.3721 Å, the 4°–84° coverage provides plenty of structural Bragg peaks but also opens up the possibility of looking for scattering from non-ferromagnetic ordering. This is in contrast to the majority of studies that appear to have a lower cut-off just below the (100) Bragg peak of the $\alpha-$phase – perhaps an unfortunate choice given the long-period antiferromagnetic ordering reported in the $MnFeP_{1-y}As_y$ system.[8] As Figure 4 shows, our low-angle measurements yielded an unexpected result: There is a clear, magnetic contribution at $2\theta \sim 8°$ that appears as the $\alpha \rightarrow \beta$ conversion is starting. It passes through a maximum near the centre of the MCT and then abruptly vanishes. It is *not* seen on re-warming, nor does it appear in any subsequent cycle. The position at its maximum intensity corresponds to a d-spacing of ~16.7 Å, and while this is about five times that of the *c*–axis distance, the peak moves to slightly lower angles on cooling, indicating that it reflects an incommensurate modulation of the magnetic structure. If we assume that this incommensurate magnetic ordering

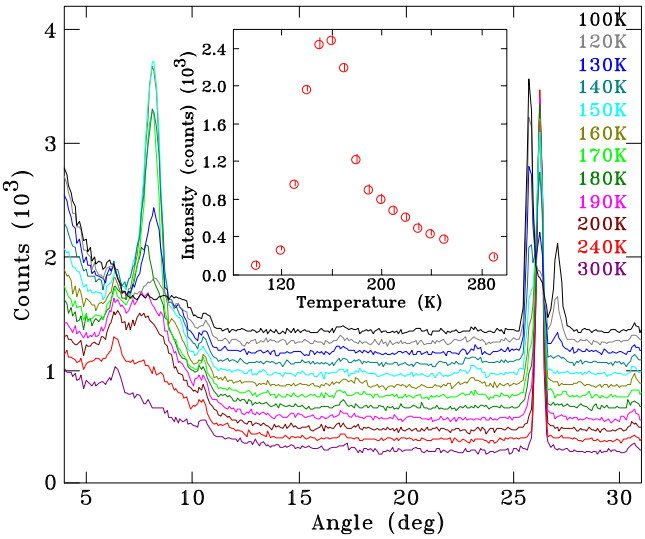

FIG. 4. Temperature dependence of the low-angle region of the neutron diffraction patterns for $Mn_{1.1}Fe_{0.9}P_{0.8}Ge_{0.2}$ taken at a wavelength of 2.3721 Å. The strong magnetic peak that develops at $2\theta \sim 8°$ is only seen during the first cooling cycle. The inset shows the intensity of the magnetic peak as a function of temperature.

of $Mn_{1.1}Fe_{0.9}P_{0.8}Ge_{0.2}$ is similar to that reported for the $MnFeP_{1-y}As_y$ system, then we find a propagation vector $q = [0, 0.37, 0]$. We identified a second magnetic peak at $2\theta \sim 23°$ with an intensity ~2% that of the primary peak. Two magnetic peaks, one of which is extremely weak, in a system with two co-existing magnetic phases is insufficient information for a formal determination of the magnetic structure.

If one compares the evolution of the magnetic intensity in Figure 4 with that of the phase fraction for the $\beta-$phase on first cooling in Figure 2, it is clear that the magnetic feature appears *before* the $\beta-$phase does, and grows rapidly even as the $\alpha-$phase is transforming. The rapid drop in intensity tracks the final loss of the $\alpha-$phase, but it proceeds to completion – the magnetic signal is completely gone by 100 K – whereas ~15 wt.% of the $\alpha-$phase survives to 4 K. Thus the loss of the magnetic feature must reflect a *change* in the $\alpha-$phase and not just its transformation into the $\beta-$phase. We therefore suggest that there may be a magnetic driver to the irreversible change seen on first cooling. For further insights we turn to first-principles DFT calculations.

In $Mn_{1.1}Fe_{0.9}P_{0.8}Ge_{0.2}$, the Mn-P(Ge) and Fe-P(Ge) layers alternate along the $c-$axis, with the magnetic ions in each layer forming a triangular network. DFT calculations show that the inter-atom exchange interactions are very different in the α and β phases. The Fe-Mn exchange interactions are similar and positive (~0.9 mRy) in both phases, while the nearest neighbour Fe-Fe exchange interactions within the Fe-P(Ge) layers are negative and about −0.3 mRy (Figure 5). By contrast, the nearest neighbour Mn-Mn exchange interactions within the Mn-P(Ge) layer are negative (−0.3 mRy) in the $\alpha-$phase and positive (+0.3 mRy) in the $\beta-$phase (Figure 5). Negative (*i.e.* antiferromagnetic AF) Mn-Mn exchange on a triangular network leads to frustration and either suppressed or complex magnetic ordering (such as the long-period AF modulation seen on first cooling). Expanding along the $a-$axis leads to positive Mn-Mn exchange and long-ranged ferromagnetic order. The gain in magnetic energy drives the $\alpha \rightarrow \beta$ MCT. The transformation reverses when the magnetic order is lost on heating through T_c leading to the conventional MCT behaviour.

Since the P and Ge are randomly distributed between the 1*a* and 2*c* sites, the local Mn-Mn separation depends on the specific local mix of P and Ge nearest neighbours. These local structural variations couple to the magnetic behaviour through fluctuations in the interatomic distances. A wide range of local configurations are possible and the specific arrangements in the as-made material will be optimised at the (high temperature) preparation conditions. However, during the magnetically driven $\alpha \rightarrow \beta$ MCT, some subset of these local configurations with low activation barriers may readjust, trading local strain energy for a global gain in magnetic energy, and if these changes are stable above 300 K they would account for the observed irreversible change in the MCT and the 0.13(1)% strain observed in the neutron diffraction data. The local adjustments favour ferromagnetic ordering and thus they both move the MCT transition up in temperature, and suppress the long-period AF modulation. In this view, the local two-level systems are driven by a competition between strain and magnetic energies, rather than being simply "high" and "low" temperature configurations,[10] but the result is essentially the same.

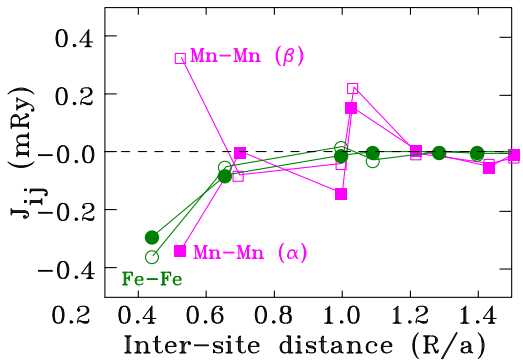

FIG. 5. The exchange coupling parameters for Mn-Mn (square) and Fe-Fe (circle) for the first six coordination shells in the *ab*-plane as a function of the inter-site distance in units of the planar lattice constant, *a*. The solid and open symbols are for the α and β phases, respectively.

IV. CONCLUSIONS

DFT calculations show that the anisotropic expansion at the $\alpha \rightarrow \beta$ MCT in $Mn_{1.1}Fe_{0.9}P_{0.8}Ge_{0.2}$ is driven by the distance dependence of the nearest neighbour Mn-Mn exchange interactions within the Mn-P(Ge) *ab*–plane layers. We find that the irreversible ~55 K shift in the MCT following cycling is associated with the development of 0.13(1)% strain and the suppression of long-period incommensurate AF ordering. We argue that small, local atomic displacements occur during the first passage through the MCT and optimise magnetic energy at the expense of strain energy, reducing the frustrated AF interactions and stabilising long-ranged ferromagnetic order. These configurational changes survive both cycling to room temperature and cycling through the MCT.

ACKNOWLEDGMENTS

Financial support for this work was provided by: the Natural Sciences and Engineering Research Council of Canada, the Fonds Québécois de la Recherche sur la Nature et les Technologies, and the The National Natural Science Foundation of China (51671006). L.M.D.C. died in January 2010.

[1] K. A. Gschneidner, Jr., V. K. Pecharsky, and A. O. Tsokol, Rep. Prog. Phys. **68**, 1479 (2005).
[2] E. Brück, in *Handbook of Magnetic Materials, Vol. 17*, edited by K. H. J. Buschow (Elsevier Science, 2007), pp. 235–291.
[3] O. Tegus, B. Li-Hong, and S. Lin, Chinese Physics B **22**, 037506 (2013).
[4] L. Zhang, O. Može, K. Prokeš, O. Tegus, and E. Brück, J. Magn. Magn. Mater. **290-291**(1), 679 (2005).
[5] D. T. Cam Thanh, E. Brück, O. Tegus, J. C. P. Klaasse, T. J. Gortenmulder, and K. H. J. Buschow, J. Appl. Phys. **99**, 08Q107 (2006).
[6] X. B. Liu, Z. Altounian, D. H. Ryan, M. Yue, Z. Li, D. Liu, and J. Zhang, J. Appl. Phys. **105**, 07A920 (2009).
[7] R. Zach, M. Guillot, and R. Fruchart, J. Magn. Magn. Mater. **89**, 221 (1990).
[8] M. Bacmann, J.-L. Soubeyroux, R. Barrett, D. Fruchart, R. Zach, S. Niziol, and R. Fruchart, J. Magn. Magn. Mater. **134**, 59 (1994).
[9] W. Dagula, O. Tegus, B. Fuquan, L. Zhang, P. Z. Si, M. Zhang, W. S. Zhang, E. Brück, F. R. de Boer, and K. H. J. Buschow, IEEE Trans. Magn. **41**, 2778 (2005).
[10] X. F. Miao, L. Caron, Z. Gercsi, A. Daoud-Aladine, N. H. van Dijk, and E. Brück, Appl. Phys. Lett. **107**, 042403 (2015).
[11] A. Bartok, M. Kustov, L. F. Cohen, A. Pasko, K. Zehani, L. Bessais, F. Mazaleyrat, and M. LoBue, J. Magn. Magn. Mater. **400**, 333 (2016).
[12] M. Yue, Z. Q. Li, X. B. Liu, H. Xu, D. M. Liu, and J. X. Zhang, J. Alloys Compds **493**, 22 (2010).
[13] A. C. Larson and R. B. V. Dreele, "General structure analysis system (gsas)," Report LAUR 86-748 (Los Alamos National Lab., 1994).
[14] B. H. Toby, J. Appl. Crystal. **34**, 210 (2001).
[15] A. I. Liechtenstein, M. I. Katsnelson, V. P. Antropov, and V. A. Gubanov, J. Magn. Magn. Mater. **67**, 65 (1987).
[16] O. K. Andersen, Phys. Rev. B **12**, 3060 (1975).
[17] M. Methfessel, M. van Schilfgaarde, and R. A. Casali, *Electronic Structure and Physical Properties of Solids: The Use of LMTO Method*, edited by H. Dreysse (Springer, Berlin, 2000).
[18] M. van Schilfgaarde and V. P. Antropov, J. Appl. Phys. **85**, 4827 (1999).
[19] D. Liu, M. Yue, J. Zhang, T. M. McQueen, J. W. Lynn, X. Wang, Y. Chen, J. Li, R. J. Cava, X. Liu, Z. Altounian, and Q. Huang, Phys. Rev. B **79**, 014435 (2009).